Experimental Study of Construction Mechanism of $V(z)$ Curves Obtained by Line-Focus-Beam Acoustic Microscopy

Yuu Ono, *Member, IEEE*, and Jun-ichi Kushibiki, *Member, IEEE*

***Abstract*—The propagation characteristics, viz., phase velocity and attenuation, of leaky surface acoustic waves (LSAWs), excited on the water/sample boundary, are obtained through analyzing the $V(z)$ curves measured by line-focus-beam acoustic microscopy. However, different values of these characteristics are obtained, depending upon different ultrasonic devices and operating frequencies employed. The construction mechanism of $V(z)$ curves was investigated experimentally by measuring the amplitude and phase for Teflon to provide an understanding of the device performance for velocity measurements. A $V(z)$ curve measured for Teflon, on which no leaky waves are excited when water is the coupling medium, can be used for the characteristic device response, depending only upon the device parameters and the operating frequencies. From the investigation of the ultrasonic device and the frequency dependences of the characteristic device responses, the phase gradient was found to be directly related to values of measured LSAW velocities. From this result, apparent frequency dependences in LSAW velocity measurements are explained quantitatively for a specimen of gadolinium gallium garnet.**

I. Introduction

Line-focus-beam (LFB) acoustic microscopy [1] can be used to measure the elastic properties of solid materials. It has been applied to characterize various materials for electronic devices such as surface acoustic wave (SAW), semiconductor and optoelectronic devices; and it has become recognized as a unique and useful method for material characterization [1]–[16].

Characterization is made by measuring the propagation characteristics, viz., phase velocity and attenuation, of leaky surface acoustic waves (LSAWs) excited on the boundary between a specimen and the water couplant through $V(z)$ curve analysis. The $V(z)$ curves are the transducer outputs recorded by changing the distance z between the LFB ultrasonic device and the specimen. Development of precision mechanical-translation stages used in the LFB system and stabilization of the temperature environment of the system were conducted to improve the measurement accuracy [17], [18]. The typical system thus has attained the relative accuracy of LSAW velocity measurements, which are mainly used for characterization, to better than $\pm 0.002\%$ at a chosen point of a specimen and $\pm 0.005\%$ for two-dimensional (180 mm $\times$ 180 mm) measurements [18]. However, different measured values have resulted from different ultrasonic devices and at different ultrasonic frequencies. Because it is necessary to have absolute values for such applications as determinations of the elastic constants of bulk and thin film materials [3], [4], [7], [9], [10], a method of calibrating the LFB system using standard specimens has been proposed [19], [20]. On the other hand, the absolute value of LSAW velocity measured by LFB acoustic microscopy has been discussed using theoretically calculated $V(z)$ curves [9], [10], [21]. But the effects due to the assumption and approximation in the theoretical calculations have not been investigated sufficiently. Therefore, the causes of the differences of the measured values have not been clarified. It is very important to investigate the causes, in order to discuss the absolute accuracy of the system, to improve and develop the system with higher accuracy, and to design the desired ultrasonic devices.

In this paper, the construction mechanism of $V(z)$ curves is examined experimentally by measuring amplitude and phase for Teflon to understand the device performance for velocity measurements. A $V(z)$ curve for Teflon, on which no leaky waves are excited, can be used for the characteristic device response $V_{\mathrm{L}}(z)$ [1], depending only upon the device parameters and the operating frequencies. Using the phase information of this $V(z)$ curve, the causes of the different values obtained in velocity measurements are discussed.

II. Model of $V(z)$ Curves

The LFB acoustic microscopy can measure the propagation characteristics of LSAWs excited on the water-specimen boundary by analyzing the $V(z)$ curves obtained by changing the distance z between an LFB ultrasonic device and the specimen. The measurement principle was described in detail previously [1]. Fig. 1 is a cross-sectional view of the LFB ultrasonic device containing a specimen, which shows the formation principle of the $V(z)$ curve. The coordinate system is set at the focal plane in water as shown in Fig. 1. When the specimen surface is located in the negative z region ($z < 0$), the two components (#0 and #1 shown in Fig. 1) mainly contribute to the transducer

Manuscript received August 26, 1999; accepted February 14, 2000. This work was supported in part by a Research Grant-in-Aid from the Ministry of Education, Science, Sports and Culture of Japan.

The authors are with the Department of Electrical Engineering, Tohoku University, Sendai 980-8579, Japan (e-mail: ono@ecei.tohoku.ac.jp).

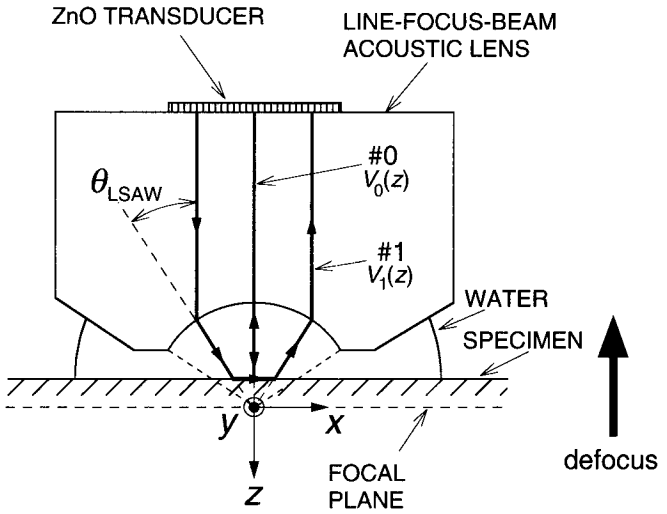

Fig. 1. Cross-sectional view of the LFB ultrasonic device and a specimen for explaining the formation principle of the $V(z)$ curves.

output. The component #0, denoted as $\mathbf{V}_0(z)$, consists of the waves reflected directly from the specimen surface, and the component #1, denoted as $\mathbf{V}_1(z)$, is associated with the waves reradiated from the specimen via LSAWs propagating at the boundary. The phasors are expressed as:

$$\mathbf{V}_0(z) = |\mathbf{V}_0(z)| \exp\{j(-2k_{\mathrm{w}}z + \phi_0)\}, \tag{1}$$

$$\mathbf{V}_1(z) = |\mathbf{V}_1(z)| \exp[j\{(-2k_{\mathrm{w}} \cos\theta_{\mathrm{LSAW}})z + \phi_1\}], \tag{2}$$

where $\theta_{\mathrm{LSAW}} = \sin^{-1}(k_{\mathrm{LSAW}}/k_{\mathrm{w}})$, and k_{LSAW} and k_{w} are the wavenumbers of the LSAWs and of the longitudinal waves in water, respectively; and ϕ_0 and ϕ_1 are the initial phases. The phasor $\mathbf{V}(z)$, the amplitude of which gives the transducer output $V(z)$, is obtained as the sum of the two phasors given by:

$$\mathbf{V}(z) = \mathbf{V}_0(z) + \mathbf{V}_1(z). \tag{3}$$

The oscillation interval Δz of the $V(z)$ curve, which depends upon the relative phase difference between the two phasors, is given by:

$$\Delta z = \frac{\pi}{k_{\mathrm{w}}\,(1 - \cos\theta_{\mathrm{LSAW}})}, \tag{4}$$

and the LSAW velocity V_{LSAW} is determined from Δz using the following:

$$V_{\mathrm{LSAW}} = \frac{V_{\mathrm{w}}}{\sqrt{1 - \left(1 - \frac{V_{\mathrm{w}}}{2f\Delta z}\right)^2}}, \tag{5}$$

where V_{w} is the velocity of longitudinal waves for water and f is the ultrasonic frequency. The attenuation of LSAW is obtained from the amplitude variation of the $V(z)$ curve. Detail of the $V(z)$ curve analysis to obtain the LSAW propagation characteristics was described earlier [1].

III. LSAW Velocity Measurements

Measurements of the $V(z)$ curves are carried out in order to investigate the performance of LFB ultrasonic devices for LSAW velocity measurements using two devices designed for 225-MHz operation, which were described in detail earlier [1]. The devices have the different ZnO-film transducer sizes of 1.73 mm × 1.50 mm (No. 1) and 1.50 mm × 1.50 mm (No. 2) with the altered transducer widths of 1.73 and 1.50 mm along the focused axis, formed on the flat ends of the cylindrical sapphire acoustic lenses with the following dimensions: the cylindrical concave surface of 1-mm radius with an aperture half-angle of 60°and a distance of 12 mm between the transducer plane and the top surface of the lens. On the cylindrical concave surface, a quarter-wavelength thick chalcogenide-glass film is fabricated as an acoustic antireflection coating layer between sapphire and water.

A (111) gadolinium gallium garnet (GGG) standard specimen [20] was used for the $V(z)$ curve measurements with LSAWs propagating in $[\overline{1}\ \overline{1}\ 2]$ direction. The specimen has sufficient thickness, approximately 3-mm thick, so that influence of the waves, reflected from the back surface of the specimen, on velocity measurements [22], [23] can be avoided.

The laser interferometer is used to determine the distance z accurately in the $V(z)$ curve measurements in the recent LFB system [18]. However, determination of z is made by the number of pulses for the stepping motor to drive the vertical translation stage (z-stage). Therefore, the z-stage positioning errors were corrected by the method using ultrasonic plane waves developed previously [24], to eliminate the influence of the positioning error on measurement accuracy of the velocity measurements.

A. Ultrasonic Device Dependence

The $V(z)$ curves measured for the GGG specimen with the two LFB ultrasonic devices at 225 MHz are shown in Fig. 2. They are significantly different in shape; the dips of the $V(z)$ curve by the No. 1 device in Fig. 2(a) were deeper than those of the $V(z)$ curve by the No. 2 device in Fig. 2(b). The difference in shape results from different acoustic fields formed on the specimen by each device [1], [25]. According to the procedure of the $V(z)$ curve analysis, the LSAW velocities were 3243.72 m/s and 3250.09 m/s from Fig. 2(a) and Fig. 2(b), respectively, where the region $z = -500$ μm to -30 μm was used for $V(z)$ curve analysis for both devices. The value of the velocity obtained by the No. 1 device was 6.37 m/s (0.20%) less than that obtained by the No. 2 device; this shows that the oscillation interval Δz of the $V(z)$ curve measured with the No. 1 device is different from that of the No. 2 device.

Moreover, LSAW velocities were obtained for different analyzing regions $z = \mathrm{Z_D}$ to -30 μm of the $V(z)$ curves, where $\mathrm{Z_D}$ is the defocus distance and was changed every 50 μm from -500 μm to -100 μm. Fig. 3 shows the results by squares and circles for the No. 1 and No. 2 devices, re-

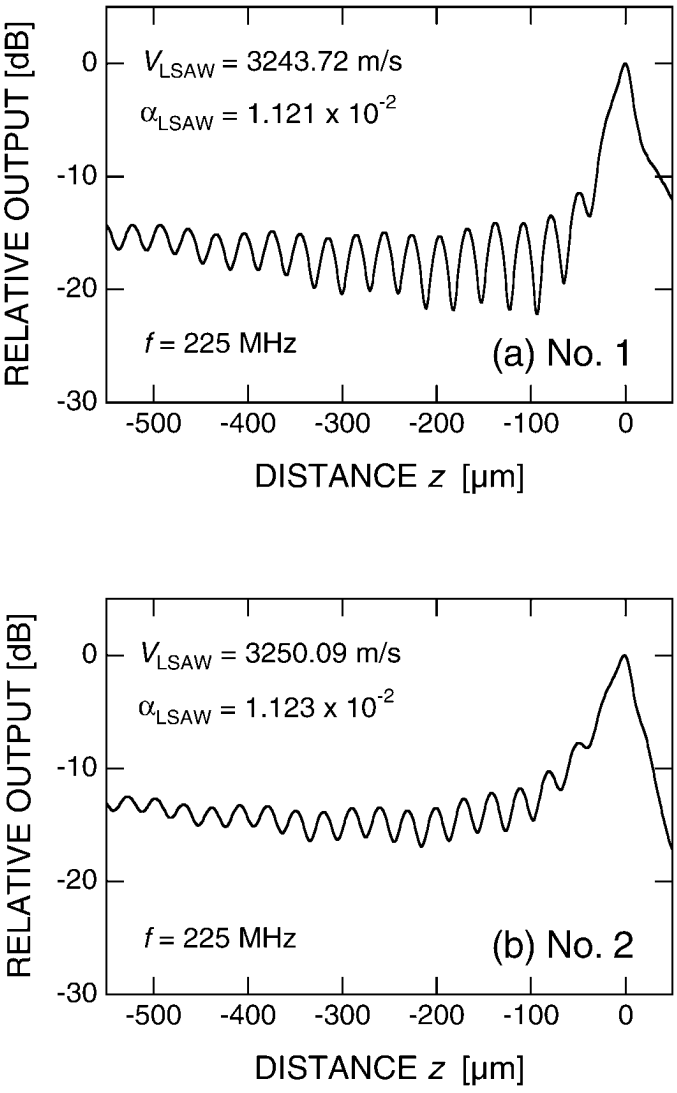

Fig. 2. $V(z)$ curves for (111) GGG measured with the two different LFB ultrasonic devices No. 1 (a) and No. 2 (b) at 225 MHz.

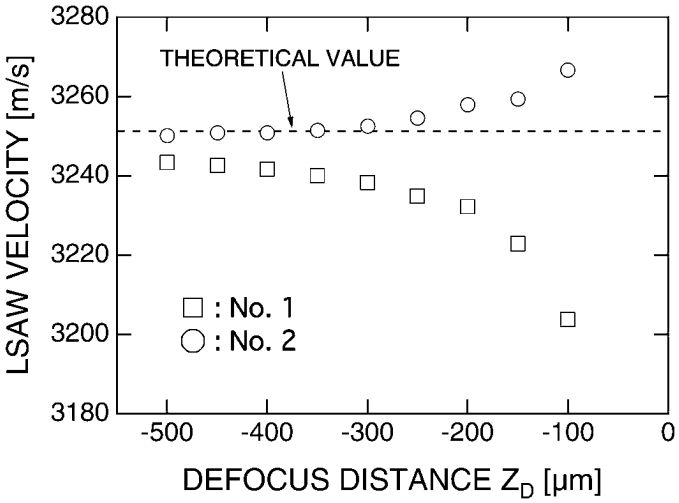

Fig. 3. LSAW velocities determined from $V(z)$ curves. Squares: obtained from the $V(z)$ curve with the No. 1 device, shown in Fig. 2(a); circles: obtained from that with the No. 2 device shown in Fig. 2(b). Analyzing region of $V(z)$ curves is $z = Z_D$ to -30 μm, where Z_D is a defocus distance.

spectively. The dashed line in Fig. 3 is the theoretical value of the LSAW velocity for (111) GGG with $[\overline{1}\overline{1}2]$ propagation at 23°C, which was calculated to be 3251.27 m/s by the analytical procedure of Campbell and Jones [26] using the physical constants of GGG [20] and those of water [27], [28]. The different values resulted from the different analyzing regions even when processed for the same $V(z)$ curve. When the analyzing region becomes shorter, the obtained value becomes smaller than the theoretical value for the No. 1 device, but greater for the No. 2 device, and the differences of the analyzed regions near the focal point ($z = 0$) influence more greatly the obtained values. This result shows that the values of Δz are different among the characterization regions in the $V(z)$ curve. Hence, the obtained values of the propagation characteristics must be calibrated to have absolute values [19], [20].

B. Frequency Dependence

The $V(z)$ curves were measured for the GGG specimen in 5-MHz steps in the frequency range 100 to 300 MHz using the two LFB devices. Fig. 4 shows the $V(z)$ curves measured at 120, 160, 200, and 240 MHz, which illustrates that the shape of the $V(z)$ curves depends greatly upon the operating frequencies. The obtained LSAW velocities are plotted by squares and circles for the No. 1 and No. 2 devices, respectively, in Fig. 5, in which the region $z = -500$ μm to -30 μm was used for $V(z)$ curve analysis for all $V(z)$ curves. It is assumed that the propagation characteristics of LSAWs for the GGG specimen are not dispersive. However, the measured LSAW velocities vary apparently with the frequency, and the frequency dependence obtained with the No. 1 device is clearly different from that obtained with the No. 2 device. The maximum deviation is 13.80 m/s (0.42%) for the No. 1 device and 14.74 m/s (0.45%) for the No. 2 device in this frequency range. These frequency dependences do not result from the acoustic properties of the specimen, but from the frequency dependences in the performance of LFB ultrasonic devices.

IV. Characteristic Device Response

As described in Section II, a $V(z)$ curve is composed of two phasors, $\mathbf{V}_0(z)$ and $\mathbf{V}_1(z)$, and the oscillation interval Δz is determined by the relative phase difference between the two phasors. Therefore, the $V(z)$ curve measured for Teflon, on which no leaky waves are excited, is associated only with the component #0, namely $\mathbf{V}_0(z)$, shown in Fig. 1. It can be used as an approximated characteristic device response $V_L(z)$, depending only upon the device parameters and the operating frequencies. Using

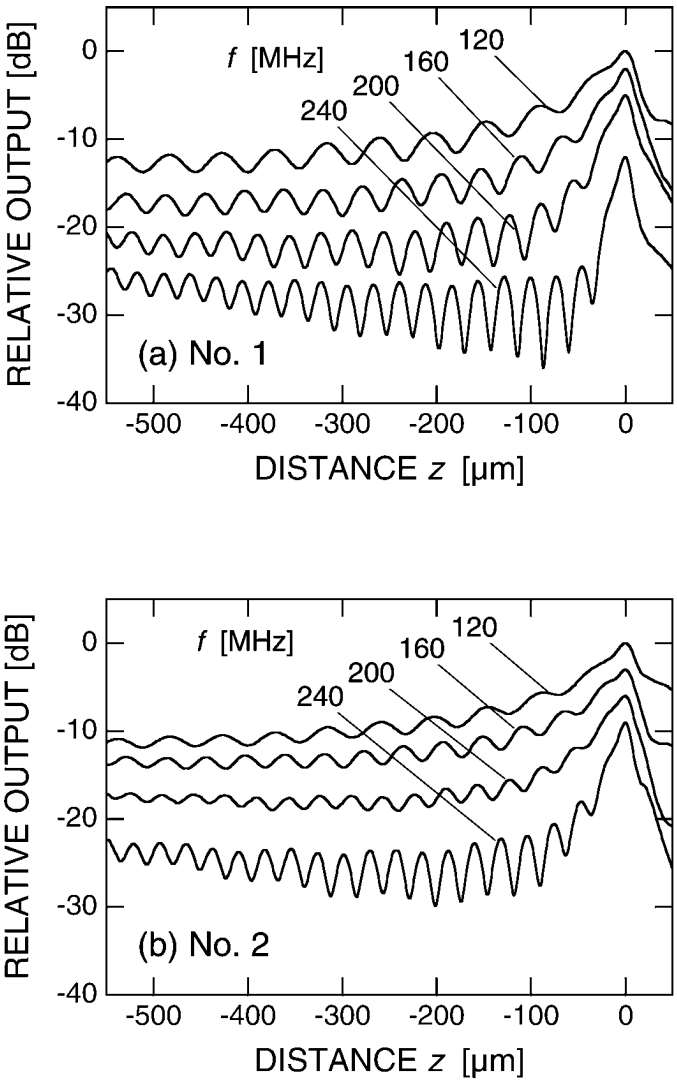

Fig. 4. $V(z)$ curves for (111) GGG measured at different frequencies. (a) No. 1 device; (b) No. 2 device.

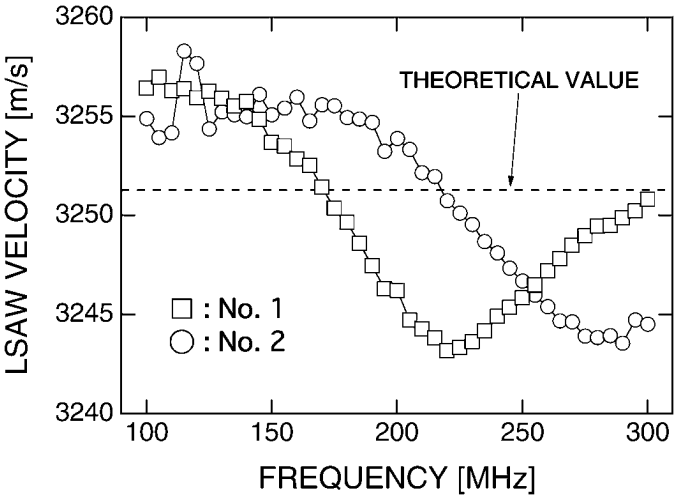

Fig. 5. LSAW velocity variations for (111) GGG measured at different frequencies.

the characteristic curves of the LFB device, namely $V_{\mathrm{L}}(z)$ curves, we investigated the causes of the difference of obtained values of LSAW velocity resulting from different LFB ultrasonic devices, different analyzing regions of the $V(z)$ curves, and different operating frequencies.

The system also can measure the phase of the RF burst pulse signals simultaneously and with high accuracy [24], [29]. The amplitude and phase of the $V_{\mathrm{L}}(z)$ curves were measured for Teflon using the two devices at 225 MHz. For examining the behavior of the phasor $\mathbf{V}_0(z)$ described in Section II, the relative phase $\Phi_{\mathrm{L}}(z)$ was obtained by subtracting the phase variation $-2k_{\mathrm{w}}z$ caused by the propagation of longitudinal waves in water from the measured phase variation, in which k_{w} is equal to $2\pi f/V_{\mathrm{w}}$, and V_{w} is obtained from the water temperature measured at the same time as the $V_{\mathrm{L}}(z)$ curve using data in the literature [27]. If the $\mathbf{V}_0(z)$ is expressed as (1), the $\Phi_{\mathrm{L}}(z)$ should be constant in the negative z region. The results are shown in Fig. 6. The shapes of the amplitude and phase are remarkably different among the two devices. The amplitude, which is maximum at the focal point ($z = 0$), has no oscillations and rapidly decreases in the negative z region. The relative phase $\Phi_{\mathrm{L}}(z)$ varies greatly around the focal point and is not always constant with z for both devices. The sign of the gradient of $\Phi_{\mathrm{L}}(z)$ with respect to z changes from positive to negative around $z = -20$ μm for the No. 1 device as shown in Fig. 6(a), and around $z = -100$ μm for the No. 2 device as shown in Fig. 6(b).

Fig. 7(a) shows the amplitude and phase of the $V_{\mathrm{L}}(z)$ curves measured at 120, 160, 200, and 240 MHz for the No. 1 device. With defocusing, the amplitude decreases more rapidly at the higher frequencies, and the phase changes greatly around the focal point ($z = 0$). In the region $z = -500$ μm to -50 μm, the phase measured at 120 MHz is almost flat; but at the other frequencies, it has positive gradients with the gradient greatest at 200 MHz. Fig. 7(b) also shows the measured amplitude and phase of $V_{\mathrm{L}}(z)$ curves for the No. 2 device. The curve shapes are different from those measured with the No. 1 device for the same frequencies, with the greatest phase gradient obtained at 240 MHz.

The measured relative phase variations $\Phi_{\mathrm{L}}(z)$ of characteristic device responses $V_{\mathrm{L}}(z)$ shown in Figs. 6 and 7 suggest that the phase variation ratio of $\mathbf{V}_0(z)$, with respect to z in the negative z region, is slightly different from $-2k_{\mathrm{w}}$ expressed in (1). This is probably due to the fact that $\mathbf{V}_0(z)$ consists of waves around the beam axis shown as #0 in Fig. 1 and due to the effects of diffraction. In Section V, we will discuss the relationship between the measured LSAW velocities and the phase variations of the $V_{\mathrm{L}}(z)$ curves.

V. Discussion

Here, the phase variation ratios of $\mathbf{V}_0(z)$ and $\mathbf{V}_1(z)$ with respect to z are defined as $k_0(z)$ and $k_1(z)$, respec-

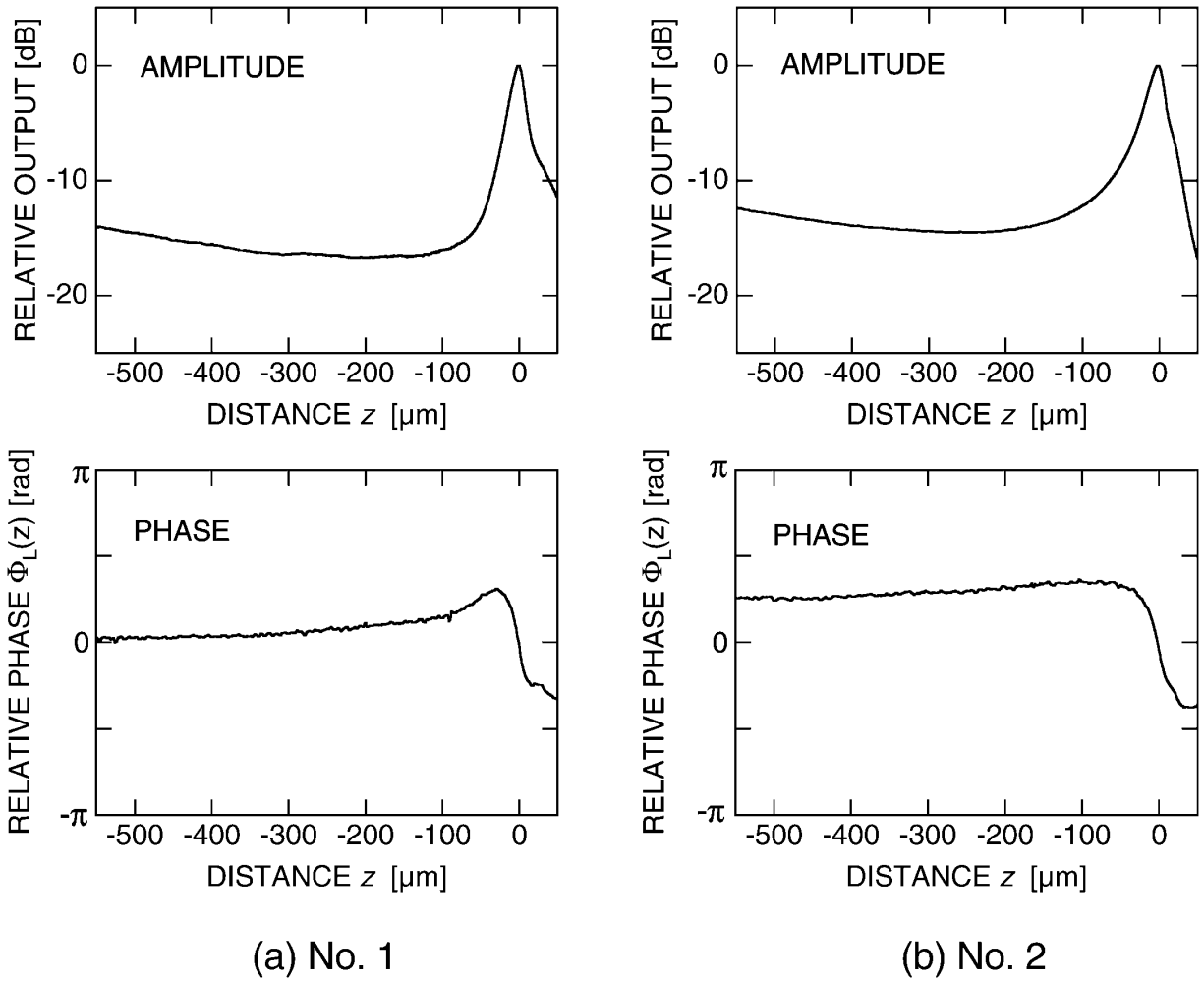

Fig. 6. Measured amplitude and phase of $V_{\mathrm{L}}(z)$ curves for Teflon at 225 MHz. (a) No. 1 device; (b) No. 2 device.

tively, and (1) and (2) are modified as follows:

$$\mathbf{V}_0(z) = |\mathbf{V}_0(z)| \exp\left\{ j \left(\int_0^z k_0(z)dz + \phi_0 \right) \right\}, \tag{6}$$

$$\mathbf{V}_1(z) = |\mathbf{V}_1(z)| \exp\left\{ j \left(\int_0^z k_1(z)dz + \phi_1 \right) \right\}. \tag{7}$$

The relative phase $\Phi_{\mathrm{L}}(z)$ obtained by subtracting the phase changes $-2k_{\mathrm{w}}z$ in the water from the phase variations of $\mathbf{V}_0(z)$ is given by:

$$\Phi_L(z) = -\int_0^z k_0(z)dz - 2k_{\mathrm{w}}z. \tag{8}$$

Therefore, $k_0(z)$ is expressed using $\Phi_{\mathrm{L}}(z)$ as

$$k_0(z) = -2k_{\mathrm{w}} - \frac{d}{dz}\Phi_{\mathrm{L}}(z). \tag{9}$$

Here, assuming $k_1(z) = -2k_{\mathrm{w}} \cos\theta_{\mathrm{LSAW}}$, as expressed in (2), the actual oscillation interval Δz_{a} of $V(z)$ curves is given by:

$$\begin{aligned} \Delta z_{\mathrm{a}} &= \frac{2\pi}{|k_0(z) - k_1(z)|} \\ &= \frac{2\pi}{2k_{\mathrm{w}}(1 - \cos\theta_{\mathrm{LSAW}}) + \frac{d}{dz}\Phi_{\mathrm{L}}(z)}, \end{aligned} \tag{10}$$

and, substituting the value of Δz_{a} into (5), the LSAW velocity V'_{LSAW} is given as:

$$\begin{aligned} V'_{\mathrm{LSAW}} &= \frac{V_{\mathrm{w}}}{\sqrt{1 - (1 - \frac{V_{\mathrm{w}}}{2f\Delta z_{\mathrm{a}}})^2}} \\ &= \frac{V_{\mathrm{w}}}{\sqrt{1 - (\cos\theta_{\mathrm{LSAW}} - \frac{1}{2k_{\mathrm{w}}}\frac{d}{dz}\Phi_{\mathrm{L}}(z))^2}}. \end{aligned} \tag{11}$$

Therefore, it is easily seen that the values of Δz_{a} and V'_{LSAW} obtained from the measured $V(z)$ curves clearly depend upon the gradient of $\Phi_{\mathrm{L}}(z)$ with respect to z. If the gradient of $\Phi_{\mathrm{L}}(z)$ is positive, the V'_{LSAW} becomes smaller than the true value of V_{LSAW}. If it is negative, V'_{LSAW} becomes greater.

Next, the gradients of the $\Phi_{\mathrm{L}}(z)$ were estimated experimentally by the least square method for each of the LFB

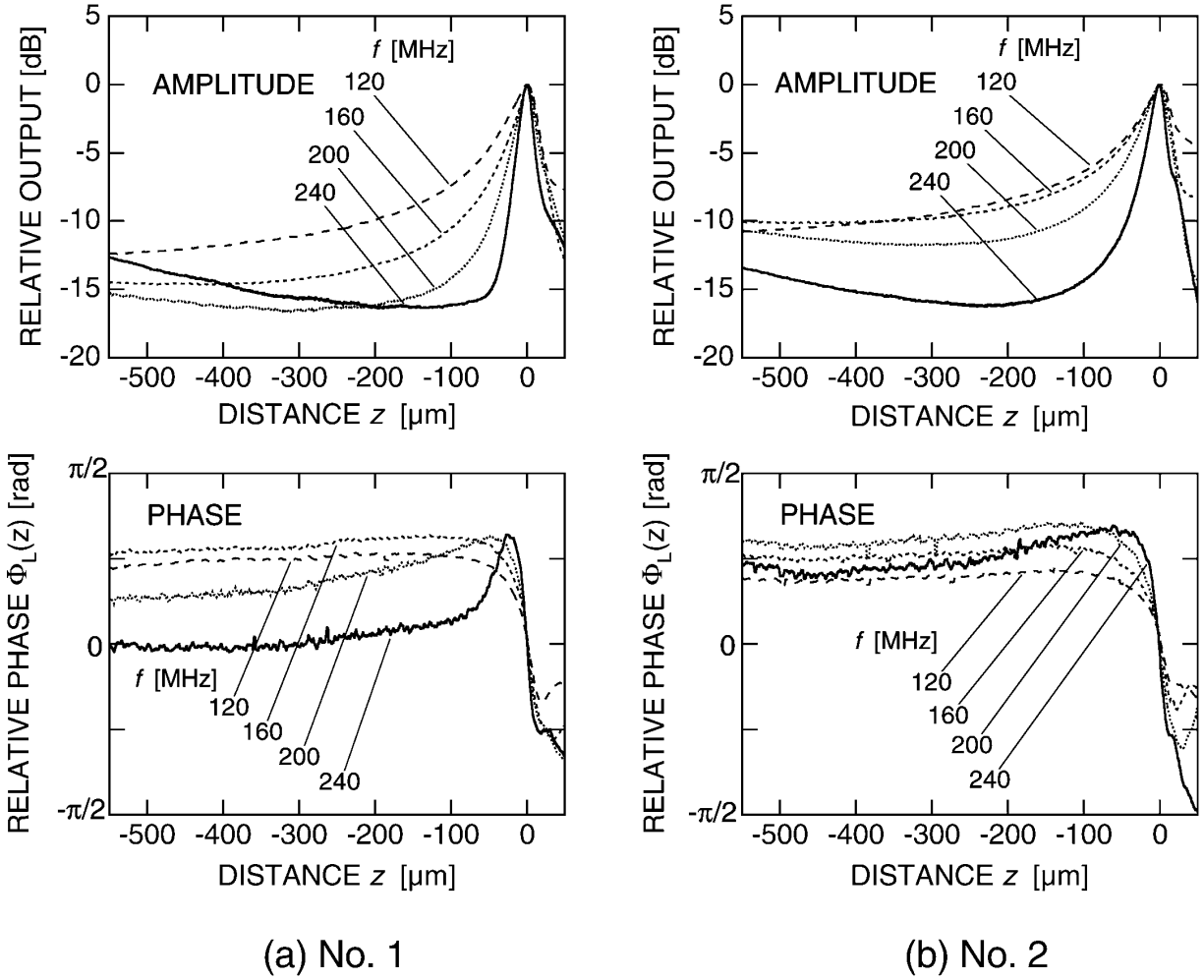

Fig. 7. Measured amplitude and phase of $V_{\mathrm{L}}(z)$ curves for Teflon at different frequencies. (a) No. 1 device; (b) No. 2 device.

devices, using the measured phases of the $V_{\mathrm{L}}(z)$ curves shown in Fig. 6. Fig. 8 shows the results by squares and circles for the No. 1 and No. 2 devices, respectively, in which the z regions used for analysis were $z = \mathrm{Z_D}$ to -30 μm, which were coincident with those used for $V(z)$ curve analysis to obtain the LSAW velocities shown in Fig. 3. For the No. 1 device, as the region used for analysis becomes shorter, the gradient of $\Phi_{\mathrm{L}}(z)$ becomes greater, suggesting that V_{LSAW} is determined to be smaller. However, for the No. 2 device, the gradient becomes smaller, suggesting that V_{LSAW} is determined to be greater. The relationships between the obtained values of the LSAW velocity and the gradient of $\Phi_{\mathrm{L}}(z)$ are plotted in Fig. 9 by squares and circles for the No. 1 and No. 2 devices, respectively. The solid line in Fig. 9 shows the calculated results of the LSAW velocities using (11), where $f = 225$ MHz, $V_{\mathrm{w}} = 1491.23$ m/s at 23°C [27], and $V_{\mathrm{LSAW}} = 3251.27$ m/s. The experimental results agree well with those calculated. Therefore, it can be said that the measured velocities strongly depend upon the phase variations of the $V_{\mathrm{L}}(z)$ curve.

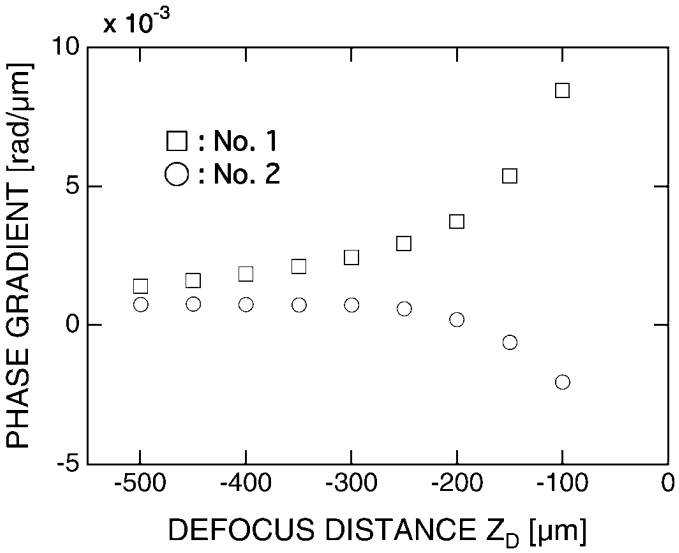

Fig. 8. Phase gradients of $V_{\mathrm{L}}(z)$ curves shown in Fig. 6. The region used for analysis of $V_{\mathrm{L}}(z)$ curves is $z = \mathrm{Z_D}$ to -30 μm, which is coincident with that used for LSAW velocities in Fig. 3.

We also discuss the frequency dependences of measured LSAW velocities shown in Fig. 5. The gradient of phase

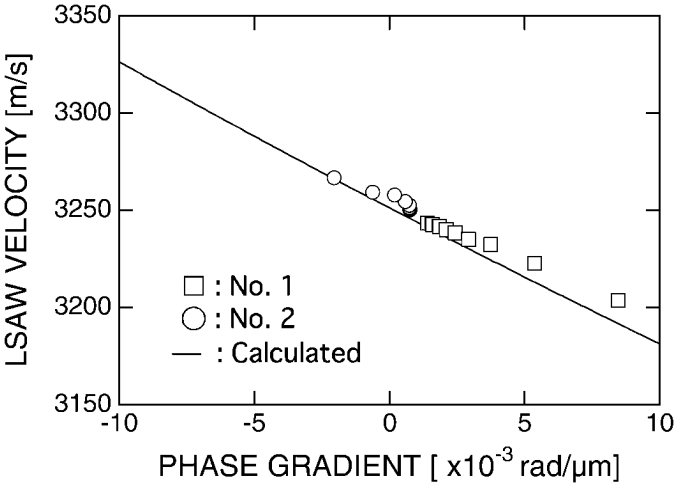

Fig. 9. Relationship between LSAW velocity and phase gradient of $V_{\mathrm{L}}(z)$ curves.

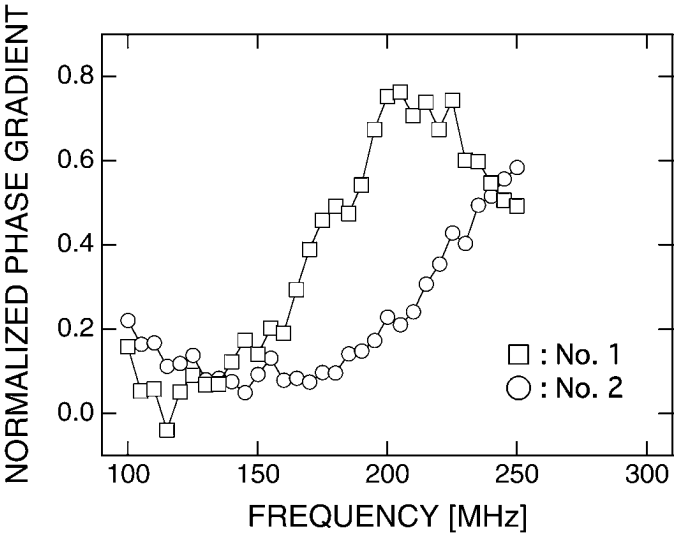

Fig. 10. Normalized phase gradient of $V_{\mathrm{L}}(z)$ curves obtained at different frequencies.

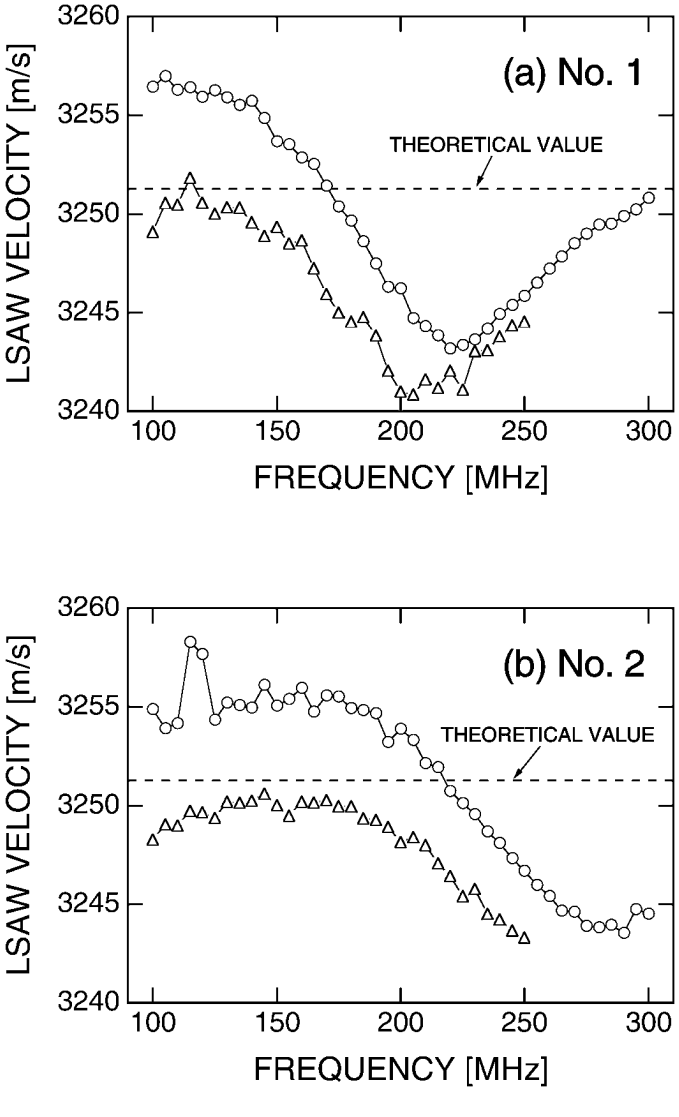

Fig. 11. Comparison of LSAW velocities obtained from measured $V(z)$ curves (circles) and calculated from normalized phase gradient of $V_{\mathrm{L}}(z)$ curves shown in Fig. 10 (triangles) at different frequencies. (a) No. 1 device; (b) No. 2 device.

$\Phi_{\mathrm{L}}(z)$ is normalized by $2k_{\mathrm{w}}$ as:

$$M_{\mathrm{L}}(z) = \frac{1}{2k_{\mathrm{w}}}\frac{d}{dz}\Phi_{\mathrm{L}}(z), \tag{12}$$

the error term in (11) is expressed as the normalized phase gradient $M_{\mathrm{L}}(z)$. Fig. 10 shows $M_{\mathrm{L}}(z)$, presented by squares for the No. 1 device and circles for the No. 2 device, obtained from the phase of $V_{\mathrm{L}}(z)$ curves measured for every 5 MHz from 100 to 250 MHz using (12), where the z region used for analysis was $z = -500$ μm to -30 μm, which was coincident with that used for the $V(z)$ curve analysis to obtain the LSAW velocities shown in Fig. 5. It is greatest at 205 MHz for the No. 1 device and 250 MHz for the No. 2 device in the frequency range used. It is predicted that the smallest value of velocity is obtained at this frequency for each device. Fig. 11 compares the frequency dependences of the LSAW velocity obtained from measured $V(z)$ curves and calculated from the phase gradient of $V_{\mathrm{L}}(z)$ curves. The calculations, plotted as triangles, were obtained from the $M_{\mathrm{L}}(z)$ shown in Fig. 10 using (11) and (12). The experimental points plotted as circles are the same as those in Fig. 5. The tendencies of the frequency dependences exhibit good agreement between the experimental and calculated results for each device. The experimental values are slightly greater than the calculated ones at all frequencies. This is mainly due to the linear approximation employed to obtain the gradient of $\Phi_{\mathrm{L}}(z)$ and to the measurement error of the coupling water temperature to obtain V_{w}.

Therefore, it is confirmed that the velocity differences, among the devices and over the frequency range considered, result from difference in performance of the devices, because different spatial frequency distributions of the acoustic fields are formed on the solid specimen by the different devices and at the different operating frequencies.

VI. Summary

The construction mechanism of the $V(z)$ curves was studied experimentally by measuring the amplitude and phase for Teflon to investigate the performance of the ultrasonic devices for LSAW velocity measurements by LFB acoustic microscopy. The $V(z)$ curves measured for Teflon, on which no leaky waves are excited, were used for the characteristic device response. From investigation of the phase variation of the characteristic device response measured with two LFB ultrasonic devices having different transducer sizes, the phase gradient is directly related to the measured values of LSAW velocities. From this result, the different values of LSAW velocities with two LFB devices and the apparent frequency dependences measured for a (111) GGG specimen are quantitatively explained.

The characteristic device response reflects the spatial frequency distributions of the acoustic fields formed on a solid specimen because it depends upon the size and shape of the ultrasonic transducer, the dimensions of the acoustic lens, the thickness and distribution of the acoustic antireflection coating layer, and the ultrasonic frequency. Therefore, the characteristic device response provides useful information for the design of the ultrasonic device [21], [30], [31] and to evaluate its performance [29]. In addition, measurement of the amplitude and phase of the ultrasonic wave is useful for investigating the origins of the measurement errors of the system and for improving the measurement accuracy of the system [24].

Acknowledgments

The authors are very grateful to Professor N. Chubachi for his helpful discussions and encouragement throughout this work, and to Dr. T. Sannomiya and Mr. T. Kobayashi for their invaluable support with the experiments.

References

[1] J. Kushibiki and N. Chubachi, "Material characterization by line-focus-beam acoustic microscope," *IEEE Trans. Sonics Ultrason.*, vol. SU-32, pp. 189–212, Mar. 1985.

[2] J. Kushibiki and N. Chubachi, "Acoustic microscopy for materials characterization," in *Proc. Ultrasonics Int. 91 Conf.*, Butterworth-Heinemann: Oxford, 1991, pp. 1–13.

[3] J. Kushibiki, T. Ueda, and N. Chubachi, "Determination of elastic constants by LFB acoustic microscope," in *Proc. IEEE Ultrason. Symp.*, 1987, pp. 817–821.

[4] J. Kushibiki, T. Ishikawa, and N. Chubachi, "Cut-off characteristics of leaky Sezawa and pseudo-Sezawa wave modes for thin-film characterization," *Appl. Phys. Lett.*, vol. 57, pp. 1967–1969, Nov. 1990.

[5] P. J. Burnett, G. A. D. Briggs, S. M. Al-Shukri, J. F. Duffy, and R. M. De La Rue, "Acoustic properties of proton-exchanged $LiNbO_3$ studied using the acoustic microscopy $V(z)$ technique," *J. Appl. Phys.*, vol. 60, pp. 2517–2522, Oct. 1986.

[6] M. Obata, H. Shimada, and T. Mihara, "Stress dependence of leaky surface wave on PMMA by line-focus-beam acoustic microscope," *Exper. Mech.*, vol. 30, pp. 34–39, Mar. 1990.

[7] T. Mihara and M. Obata, "Elastic constant measurement by using line-focus-beam acoustic microscope," *Exper. Mech.*, vol. 32, pp. 30–33, Mar. 1992.

[8] C. K. Jen, C. Neron, A. Shang, K. Abe, L. Bonnell, and J. Kushibiki, "Acoustic characterization of silica glasses," *J. Amer. Ceram. Soc.*, vol. 76, pp. 712–716, Mar. 1993.

[9] Y. C. Lee, J. O. Kim, and J. D. Achenbach, "Acoustic microscopy measurement of elastic constants and mass density," *IEEE Trans. Ultrason., Ferroelect., Freq. Contr.*, vol. 42, pp. 253–264, Mar. 1995.

[10] J. D. Achenbach, J. O. Kim, and Y.-C. Lee, "Measuring thin-film elastic constants by line-focus acoustic microscopy," in *Advances in Acoustic Microscopy*. vol. 1, A. Briggs, Ed. New York: Plenum, 1995, pp. 153–208.

[11] J. Kushibiki, H. Takahashi, T. Kobayashi, and N. Chubachi, "Quantitative evaluation of elastic properties of $LiTaO_3$ crystals by line-focus-beam acoustic microscopy," *Appl. Phys. Lett.*, vol. 58, pp. 893–895, Mar. 1991.

[12] J. Kushibiki, H. Takahashi, T. Kobayashi, and N. Chubachi, "Characterization of $LiNbO_3$ crystals by line-focus-beam acoustic microscopy," *Appl. Phys. Lett.*, vol. 58, pp. 2622–2624, June 1991.

[13] J. Kushibiki, T. Kobayashi, H. Ishiji, and N. Chubachi, "Elastic properties of 5-mol % MgO doped $LiNbO_3$ crystals measured by line focus beam acoustic microscopy," *Appl. Phys. Lett.*, vol. 61, pp. 2164–2166, Nov. 1992.

[14] J. Kushibiki, H. Ishiji, T. Kobayashi, N. Chubachi, I. Sahashi, and T. Sasamata, "Characterization of 36°YX-$LiTaO_3$ wafers by line-focus-beam acoustic microscopy," *IEEE Trans. Ultrason., Ferroelect., Freq. Contr.*, vol. 42, pp. 83–90, Jan. 1995.

[15] J. Kushibiki, M. Miyashita, and N. Chubachi, "Quantitative characterization of proton-exchanged layers in $LiTaO_3$ optoelectronic devices by line-focus-beam acoustic microscopy," *IEEE Photon. Technol. Lett.*, vol. 8, pp. 1516–1518, Nov. 1996.

[16] J. Kushibiki and M. Miyashita, "Characterization of domain-inverted layers in $LiTaO_3$ by line-focus-beam acoustic microscopy," *Jpn. J. Appl. Phys.*, vol. 36, pp. 959–961, July 1997.

[17] T. Kobayashi, J. Kushibiki, and N. Chubachi, "Improvement of measurement accuracy of line-focus-beam acoustic microscope system," in *Proc. IEEE Ultrason. Symp.*, 1992, pp. 739–742.

[18] J. Kushibiki and Y. Ono, "Development of the line-focus-beam ultrasonic material characterization system," submitted for publication.

[19] J. Kushibiki, T. Wakahara, T. Kobayashi, and N. Chubachi, "A calibration method of the LFB acoustic microscope system using isotropic standard specimens," in *Proc. IEEE Ultrason. Symp.*, 1992, pp. 719–722.

[20] J. Kushibiki and M. Arakawa, "A method for calibrating the line-focus-beam acoustic microscopy system," *IEEE Trans. Ultrason., Ferroelect., Freq. Contr.*, vol. 45, pp. 421–430, Mar. 1998.

[21] A. Atalar, H. Köymen, A. Bozkurt, and G. Yaralioğlu, "Lens geometries for quantitative acoustic microscopy," in *Advances in Acoustic Microscopy*. vol. 1, A. Briggs, Ed. New York: Plenum, 1995, pp. 117–151.

[22] J. Kushibiki, Y. Ohashi, and M. Arakawa, "Precise velocity measurements for thin specimens by line-focus-beam acoustic microscopy," *Jpn. J. Appl. Phys.*, vol. 38, pp. 89–91, Jan. 1999.

[23] J. Kushibiki and Y. Ohashi, "Theoretical and experimental considerations on line-focus-beam acoustic microscopy for thin specimens," *Jpn. J. Appl. Phys.*, vol. 38, pp. 342–344, Mar. 1999.

[24] Y. Ono, J. Kushibiki, and N. Chubachi, "A measurement method of moving characteristics of precision mechanical-translation stages using ultrasonic plane waves and its application to a line-focus-beam acoustic microscopy system," *J. IEICE Trans. A*, vol. J78-A, pp. 279–286, Mar. 1995.

[25] J. Kushibiki, Y. Matsumoto, and N. Chubachi, "Effects of acoustic field distribution of line-focus-beam on $V(z)$ curves," in *Rep. Spring Meeting Acoust. Soc. Jpn.*, pp. 661–662, Mar. 1983.

[26] J. J. Campbell and W. R. Jones, "Propagation of surface waves at the boundary between a piezoelectric crystal and a fluid medium," *IEEE Trans. Sonics Ultrason.*, vol. SU-17, pp. 71–76, Apr. 1970.

[27] W. Kroebel and K.-H. Mahrt, "Recent results of absolute sound velocity measurements in pure water and sea water at atmospheric pressure," *Acustica*, vol. 35, pp. 154–164, 1976.

[28] G. S. Kell, "Density, thermal expansivity, and compressibility of liquid water from 0° to 150°C: Correlations and tables for atmospheric pressure and saturation reviewed and expressed on

1968 temperature scale," *J. Chem. Eng. Data*, vol. 20, pp. 97–105, 1975.
[29] Y. Sugawara, J. Kushibiki, and N. Chubachi, "Performance of concave transducers in acoustic microscopy," in *Proc. IEEE Ultrason. Symp.*, 1988, pp. 751–756.
[30] Y. Sugawara, J. Kushibiki, and N. Chubachi, "Theoretical analysis on acoustic fields formed by focusing devices in acoustic microscopy," in *Proc. IEEE Ultrason. Symp.*, 1986, pp. 783–788.
[31] C.-H. Chou, B. T. Khuri-Yakub, and G. S. Kino, "Lens design for acoustic microscopy," *IEEE Trans. Ultrason., Ferroelect., Freq. Contr.*, vol. 35, pp. 464–469, July 1988.

Yuu Ono (M'99) was born in Yamanashi Prefecture, Japan, on March 18, 1967. He received the B.S., M.S., and Ph.D. degrees in electrical engineering from Tohoku University, Sendai, Japan, in 1990, 1992, and 1995, respectively.

Since 1995, he has been a research associate at the Department of Electrical Engineering, Faculty of Engineering, Tohoku University. He has been studying the development of the line-focus-beam acoustic microscopy system and its application to material characterization.

Dr. Ono is a member of the Institute of Electronics, Information and Communication Engineers of Japan; the Acoustical Society of Japan; and the Japan Society of Applied Physics.

Jun-ichi Kushibiki (M'83) was born in Hirosaki, Japan, on November 23, 1947. He received the B.S., M.S., and Ph.D. degrees in electrical engineering from Tohoku University, Sendai, Japan, in 1971, 1973, and 1976, respectively.

In 1976, he became Research Associate at the Research Institute of Electrical Communication, Tohoku University. In 1979, he joined the Department of Electrical Engineering, Faculty of Engineering, Tohoku University, where he was Associate Professor from 1988 to 1993 and became Professor in 1994. He has been studying ultrasonic metrology, especially acoustic microscopy and its applications, and has established a method of material characterization by LFB acoustic microscopy. He also has been interested in biological tissue characterization in the higher frequency range, applying both bulk and acoustic microscopy techniques.

Dr. Kushibiki is a member of the Acoustical Society of America; the Institute of Electronics, Information, and Communication Engineers of Japan; the Institute of Electrical Engineers of Japan; the Acoustical Society of Japan; and the Japan Society of Ultrasonics in Medicine.